Performance analysis and evaluation of direct phase measuring deflectometry

Ping Zhao[1], Nan Gao[1], Zonghua Zhang[1,2,*], Feng Gao[2], Xiangqian Jiang[2]

[1] School of Mechanical Engineering, Hebei University of Technology, Tianjin, 300130, China

[2] Centre for Precision Technologies, University of Huddersfield, Huddersfield, HD1 3DH, UK

*Correspondence: zhzhang@hebut.edu.cn; zhzhangtju@hotmail.com

Abstract: Three-dimensional (3D) shape measurement of specular objects plays an important role in intelligent manufacturing applications. Phase measuring deflectometry (PMD)-based methods are widely used to obtain the 3D shapes of specular surfaces because they offer the advantages of a large dynamic range, high measurement accuracy, full-field and noncontact operation, and automatic data processing. To enable measurement of specular objects with discontinuous and/or isolated surfaces, a direct PMD (DPMD) method has been developed to build a direct relationship between phase and depth. In this paper, a new virtual measurement system is presented and is used to optimize the system parameters and evaluate the system's performance in DPMD applications. Four system parameters are analyzed to obtain accurate measurement results. Experiments are performed using simulated and actual data and the results confirm the effects of these four parameters on the measurement results. Researchers can therefore select suitable system parameters for actual DPMD (including PMD) measurement systems to obtain the 3D shapes of specular objects with high accuracy.

Keywords: Error analysis; performance evaluation; simulation; direct phase measuring deflectometry; 3D shape measurement; specular object.

1. Introduction

Three-dimensional (3D) shape measurement techniques for diffuse objects have been widely used in manufacturing industries [1,2] in applications such as quality inspection and reverse engineering. Full-field fringe projection techniques [2-6] have been widely used to obtain the 3D shapes of these diffuse objects because they offer the advantages of noncontact operation, full-field acquisition, high accuracy, and fast, automatic data processing. Along with diffuse objects, specular surfaces also have a wide range of applications in various fields [7], including new energy generation, illumination, and aerospace and biomedical engineering. Therefore, to guarantee the technical performance and the visual appearance of specular products, it is essential to develop a method for measurement of specular surfaces. Phase measuring deflectometry (PMD) methods have been widely applied to provide accurate shape measurements because of advantages that include high dynamic range, full-field acquisition, noncontact operation, high accuracy and low cost [8-9].

In general, PMD uses the phase information that is calculated from reflected fringe patterns to obtain the slope data of the specular objects to be measured. A 3D shape is then reconstructed using two-dimensional (2D) local slope integration. Su et al. [8,9] proposed a software-configurable optical test system for optical surface measurement and added an auxiliary lens to perform both mid- and high-spatial-frequency optical surface metrology. Huang et al [10] built a monoscopic fringe reflectometric system using only one liquid crystal display (LCD) screen and one digital camera to perform dynamic shape measurements. Tang et al. [11,12] measured the 3D shape of an

aspheric mirror using the reflected rays and a 'dummy paraboloid'. Xiao et al [13] proposed a flexible PMD system calibration method based on use of a markerless flat mirror. However, deviations during calculation of the slope will lead to error accumulation in the height calculations. To remove the slope integration requirements, many methods have been developed to build a relationship between slope and depth. Petz et al. [14] proposed a deflectometry system using one camera and two reference grating planes for pointwise computation of the absolute 3D object coordinates, while Guo et al. [15] proposed a least-squares light incident-light tracking technique for specular surface measurement. During their measurement processes, both methods [14,15] need to shift their LCD screens to different positions to determine the orientation of the incident ray relative to the slope, which leads to instability and thus inaccurate measurement results. Knauer et al. [16] proposed a stereo deflectometry method to obtain the absolute slope and height based on calibration of the normals at the same point for two cameras. Feng et al. [17] built a dual-camera fringe projection system to reconstruct dynamic 3D shapes by combining standard three-step phase-shifting fringe patterns with a digital speckle image. However, calibration processes in dual-camera systems are complex. Recently, Huang et al. [18] presented a method for simultaneous estimation of the height and the slopes of a surface under test in PMD based on use of a mathematical model and optimization of the orientation of the screen geometry after pre-calibration of the PMD system.

To solve the above problems and build a stable measurement system, a direct PMD (DPMD) system [19] has been developed to form a relationship between the phase and the depth directly without the need for a slope integration procedure. The proposed system consists of two LCD screens, one beam splitter (BS) plate and one charge-coupled device (CCD) camera. The measurement results and the system performance are affected by the arrangements of the relevant component locations and the ways in which the parameters are set in a 3D measuring system [20]. However, to the best of our knowledge, there are no published works in the literature on evaluation of system performance and analysis of the effects of the system parameters on the measurement results in PMD. While this paper analyzes the system parameters quantitatively for DPMD, the proposed method can be applied to general PMD systems.

The next Section describes the principle and the configuration of the developed DPMD system. The simulated DPMD measurement system is introduced in Section 3. Section 4 provides an analysis of the effects of the system parameters on the measurement results. Experimental results when using the actual system are provided in Section 5 and some concluding remarks are given in Section 6.

2. Principle of direct phase measuring deflectometry

A schematic diagram of the developed DPMD system is shown in Fig. 1. This system consists of two LCD screens, a CCD camera, and a BS plate. LCD_1' represents a virtual image of screen LCD_1 via the BS. Screens LCD_2 and LCD_1' are both parallel to the reference plane R. h is the height of a given point on the tested surface, d is the distance between screen LCD_1' (the virtual image of screen LCD_1) and reference plane R, and Δd is the distance between LCD_1' and LCD_2. θ' represents the angle between the normal vector of the reference plane and the incident ray from the camera, φ represents the double gradient angle of the point that is tested on the measured surface, d_L represents the physical size of a single pixel unit on the LCD screen, and ϕ_{r1}' (ϕ_{r1}) and ϕ_{m1}' (ϕ_{m1}) denote the two different absolute phases on LCD_1'. ϕ_{r2} and ϕ_{m2} denote the two different absolute phases on LCD_2. Both the absolute phases ϕ_{r1}' and ϕ_{r2} are on

the same incident ray that is reflected into the CCD camera from the mirror at the reference position. Both the absolute phases ϕ_{m1}' and ϕ_{m2} are on the same incident ray that is reflected into the CCD camera from the measured surface. ΔL_1 represents the distance between phases ϕ_{r1}' and ϕ_{m1}'.
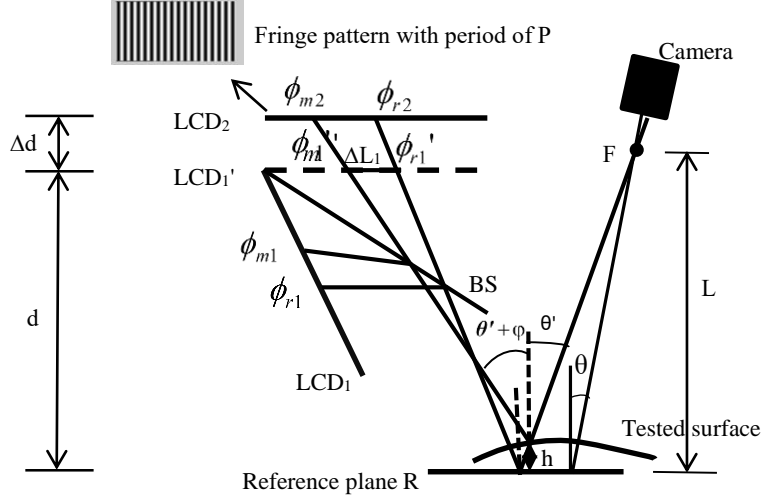

Fig. 1. Schematic diagram of the DPMD system.

Fringe patterns are generated using software and are displayed on the two LCD screens. The intensity distribution of a single displayed fringe pattern can be expressed as

$$I_0(x,y)= a(x,y)+b(x,y)\cdot\cos[\frac{2\pi}{P}\cdot x+\varphi_0(x,y)] \tag{1}$$

where $\varphi_0(x,y)$ is the phase shift term, $a(x,y)$ and $b(x,y)$ account for the background intensity and the fringe contrast, respectively, and P is the period of the displayed fringes. The fringe patterns that are displayed on screens LCD$_1$ and LCD$_2$ are reflected into the CCD camera via the surface under test and the mirror at the reference position to provide different viewpoints. After the absolute phase is calculated from the captured fringe patterns, the depth information can be obtained directly.

From the geometric relations of the DPMP measuring system shown in Fig. 1, the following equations can be derived:

$$(\phi_{r1}'-\phi_{r2}')\cdot d_L / 2\pi = \Delta d\cdot\tan\theta' \tag{2}$$

$$(\phi_{m1}'-\phi_{m2})\cdot d_L / 2\pi = \Delta d\cdot\tan(\theta'+\varphi) \tag{3}$$

$$(d+h)\cdot\tan\theta'+\Delta L_1 = (d-h)\cdot\tan(\theta'+\varphi) \tag{4}$$

$$(\phi_{r1}'-\phi_{m1}')\cdot d_L / 2\pi = \Delta L_1 \tag{5}$$

$$\phi_{r1}'=\phi_{r1} \tag{6}$$

$$\phi_{r2}'=\phi_{r2} \tag{7}$$

By combining Eqs. (2)–(7), h can be calculated as

$$h = \frac{\Delta d\cdot(\phi_{r1}-\phi_{m1})-d\cdot[(\phi_{r1}-\phi_{r2})-(\phi_{m1}-\phi_{m2})]}{(\phi_{m1}-\phi_{m2})+(\phi_{r1}-\phi_{r2})} \tag{8}$$

Equation (8) demonstrates that Δd and d affect the measurement results directly. Equation (1) shows that P influences the fringe pattern distribution and Eqs. (2)–(5) indicate that θ' affects the phase distances between ϕ_{r1} and ϕ_{r2}, ϕ_{m1} and ϕ_{m2}, and ϕ_{r1} and ϕ_{m1}. Therefore, the measurement results will be related to and affected by all the system parameters, including Δd, d, θ', and P. Because the angle θ between the optical axis of the camera and the normal vector of the reference plane is a special value of θ', which can be calculated easily from the calibration of the

camera, θ' can be replaced with θ in the system parameter analysis process. Based on the mathematical model above, a simulated DPMD measurement system is constructed in the following section.

3. Simulated DPMD measurement system

The principle of the simulated specular measurement system is based on a combination of DPMD and a pinhole imaging model. It is therefore necessary to calculate not only the geometrical relationships between the two LCD screens and the specular surface but also that between the specular surface and the CCD camera.

3.1 Projection of LCD$_2$ screen to reference plane

The purpose of calculating the projection of LCD$_2$ to reference plane R is to calculate the imaging of the fringes on LCD$_2$ in reference plane R. The geometry of the 3D imaging system is shown in Fig. 2. Plane LCD$_1$' represents the virtual imaging plane of LCD$_1$ through the plate BS, as shown in Fig. 1, and both planes LCD$_1$' and LCD$_2$ lie parallel to R. Planes LCD$_2$' and LCD$_1$" represent the virtual imaging planes (via R) of screens LCD$_2$ and LCD$_1$', respectively. Plane S is the CCD plane. OO$_S$ represents the optical axis of plane S, and the line M$_S$N$_S$ is the axis of symmetry of plane S. Line MN lies parallel to the x-axis of plane R, and both line M$_1$'N$_1$' on plane LCD$_1$' and line M$_2$N$_2$ on plane LCD$_2$ lie parallel to the x_2-axis of plane LCD$_2$. Three blue light rays are displayed and are then reflected into the CCD camera by R and two gray light rays are displayed and are reflected into the CCD camera by the test points on the plane under test.
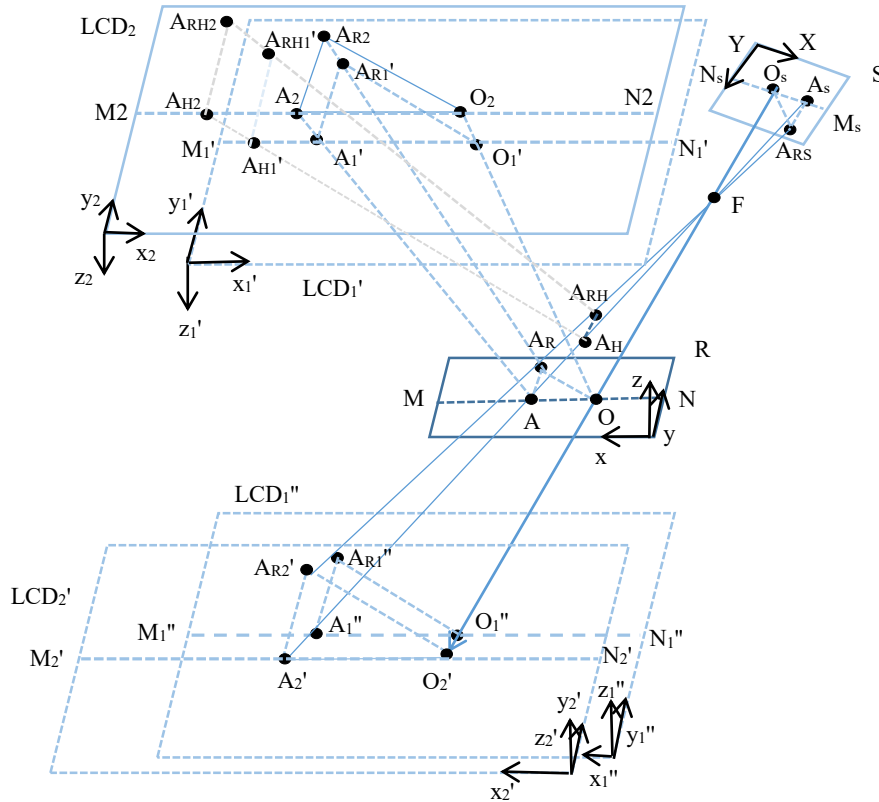

Fig. 2. Geometry of the 3D imaging system.

First, the location of the point O$_2$(x_{o2},y_{o2},0) on the plane LCD$_2$ is specified. Point O$_2$ on plane LCD$_2$ then projects light onto the point O(x_o,y_o,0) on plane R, and the line O$_2$O passes through point O$_1$'(x_{o1}',y_{o1}',0) on plane LCD$_1$'. The light is then reflected by R and is subsequently projected onto point O$_S$(X_{OS},Y_{OS},0) on plane S. Points O and O$_S$ denote the center of plane R and the imaging center of plane S, respectively. Subsequently, assuming that any point A$_{R2}$(x_2,y_2,0) other

than point O_2 on plane LCD_2 is projecting light onto point $A_R(x,y,0)$ on plane R, the line $A_{R2}A_R$ then passes through point $A_{R1}'(x_1',y_1',0)$ on plane LCD_1'. The light is then reflected by plane R and is projected onto point $A_{RS}(X_S,Y_S,0)$ on plane S. Points $A_{R2}'(x_2',y_2',0)$ and $O_2'(x_{o2}',y_{o2}',0)$ on plane LCD_2' represent the virtual imaging points of points A_{R2} and O_2 on plane LCD_2, respectively. The LCD screen resolution is given by $X_{LCD} \times Y_{LCD}$, and the physical size of a single pixel unit on the LCD screen is given by $d_L \times d_L$.

Assuming the displayed fringe patterns on LCD screen is vertical and y-axis is along the fringe direction, the height value only relates to x coordinate. Therefore, the measuring system can be simplified as 2D geometry, as shown in Fig. 3. Two blue light rays are displayed and are then reflected into the CCD camera by R and one gray light ray is displayed and reflected into the CCD camera by the test points on the plane under test. Plane H represents the plane under test. d and Δd are the distance between planes LCD_1' and $LCD2$ and the distance between planes LCD_1' and R, respectively. L represents the distance between the CCD lens center and plane R. O_SF is the focal length f of the camera lens. θ is the angle between OO_S and the normal vector of plane R. φ represents the doubled value of the gradient angle of point A_{RH} on plane H. h is the height of point A_{RH} on plane H with respect to R.
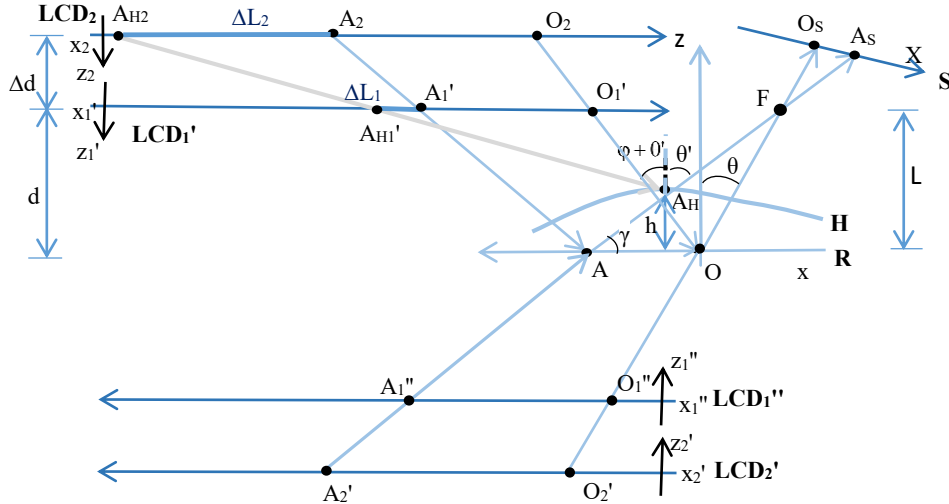

Fig. 3. Geometry of the 2D imaging system.

First, the relationship between point A_{R2} on plane LCD_2 and point A_R on plane R is calculated. Points $A_2(x_2,0,0)$, $A(x,0,0)$, and $A_S(X_S,0,0)$ are the projections of points A_{R2} to M_2N_2, A_R to MN, and A_{RS} to M_SN_S, respectively. Point $A_2'(x_2',0,0)$ on plane LCD_2' is the imaged point of point A_2 on plane LCD_2. Based on the geometric relationships shown in Fig. 3, ΔFAO is similar to $\Delta FA_2'O_2'$, $d_2=d+\Delta d$, $FO=L/\cos\theta$, and $FO_2'=(L+d_2)/\cos\theta$, and thus the following equation is obtained.

$$A_2'O_2' = \frac{L+d+\Delta d}{L} \cdot AO \tag{9}$$

The number of pixels between point A_2' and point O_2' is given by

$$N_{A_2'O_2'} = \frac{A_2'O_2'}{d_L} \tag{10}$$

Only the projected fringe areas on plane R are imaged on plane S, and thus R can be regarded as a discrete plane that consists of numerous points. The physical size of a single pixel unit on plane R is assumed to be denoted by $d_M \times d_M$. Based on the geometric relationships of $A_2'O_2'=d_L \times N_{A2'O2'}$, $AO=d_M \times N_{A2'O2'}$ and Eq. (9), the following equation is obtained.

$$d_M = \frac{L}{L + d + \Delta d} \cdot d_L \tag{11}$$

Because $A_2'O_2' = (x_2' - x_{o2}') \times d_L$ and $AO = (x - x_o) \times d_M$, then by combining Eqs. (9) and (11), the coordinate relationship between point A_2' on plane LCD2' and point A on plane R can be obtained using the following equation.

$$x_2' = (x - x_o) + x_{o2}' \tag{12}$$

The coordinate relationship between point A_2' on plane LCD2' and point A_2 on plane LCD2 is

$$x_2 = X_{LCD} - x_2' \tag{13}$$

The restriction that the fringe patterns must be parallel to the y-axis indicates that the test height is not dependent on the y value. Therefore, when the x_2-coordinate value of point A_{R2} on plane LCD$_2$ is obtained, the fringe pixel value of the point A_{R2}' on plane LCD$_2'$ can also be calculated.

3.2 Projection of LCD$_1$ screen to reference plane

Based on the geometric relationships, the angle γ between the line AA$_S$ and the plane R in Fig. 3 can be obtained using the following equation.

$$\gamma = \frac{L}{L \cdot \tan\theta + AO} \tag{14}$$

Point A_1' $(x_1', 0, 0)$ is the projection from the point $A_{R1}'(x_1', y_1', 0)$ on plane LCD$_1'$ to the line $M_1'N_1'$. The coordinate relationship between point A_1' on plane LCD$_1'$ and point $A_2(x_2, 0, 0)$ on plane LCD$_2$ is given by

$$x_1' = x_2 + \frac{\Delta d \cdot \cot\gamma}{d_L} \tag{15}$$

When the x_1'-coordinate value of point $A_{R1}'(x_1', y_1', 0)$ on plane LCD1' is obtained, the fringe pixel value of the point A_{R1}'' on plane LCD$_1''$ can then be calculated.

3.3 Projections of LCD$_1$ and LCD$_2$ to tested plane

The purpose of calculating these projections of the LCD$_1$ and LCD$_2$ screens on the tested plane is to enable calculation of the imaging of the fringes on screens LCD$_1$ and LCD$_2$ in the plane under test. In Fig. 2, it is assumed that point $A_{RH2}(x_{H2}, y_{H2}, 0)$ on screen LCD$_2$ is projecting light onto point $A_{RH}(x_H, y_H, 0)$ on plane H, and the line $A_{RH2}A_{RH}$ then passes through point $A_{RH1}'(x_{H1}', y_{H1}', 0)$ on plane LCD$_1'$. This light is then reflected by plane H and is projected onto plane S. $A_{H2}(x_{H2}, 0, 0)$ on screen LCD$_2$, $A_{H1}'(x_{H1}', 0, 0)$ on plane LCD$_1'$, and $A_H(x_H, 0, h)$ on plane H are the projections of $A_{RH2}(x_{H2}, y_{H2}, 0)$ to M_2N_2, $A_{RH1}'(x_{H1}', y_{H1}', 0)$ to $M_1'N_1'$ and $A_{RH}(x_H, y_H, h)$ to AA$_S$, respectively. The corresponding 2D geometric relationship between the planes LCD$_1'$ and LCD$_2$ and the plane under test is shown in Fig. 3.

The relationship between point A_{RH} on plane H and point A_R on plane R can be obtained using the iterative method given in [21]. This then allows the height, the gradient and the gradient angle of point A_{RH} on plane H to be obtained. Based on the geometric relationship shown in Fig. 3, $\theta' = \pi/2 - \gamma$. The distance ΔL_1 between points A_{H1}' and A_1' on plane LCD1' and the distance ΔL_2 between points A_{H2} and A_2 on plane LCD2' can then be obtained using the following equations.

$$\Delta L_1 = (d - h) \cdot \tan(\theta' + \varphi) - (d + h) \cdot \tan\theta' \tag{16}$$

$$\Delta L_2 = (d + \Delta d - h) \cdot \tan(\theta' + \varphi) - (d + \Delta d + h) \cdot \tan\theta' \tag{17}$$

The coordinate relationship between point A_{RH1}' on plane LCD$_1'$ and point A_{RH} on plane H and the additional coordinate relationship between point A_{RH2} on plane LCD$_2$ and point A_{RH} on plane H can be obtained using the following equations.

$$x_{H1}' = x_1' - \frac{\Delta L_1}{d_L} \qquad (18)$$

$$x_{H2} = x_2 - \frac{\Delta L_2}{d_L} \qquad (19)$$

When the x_{H1}' value of the point $A_{RH1}'(x_{H1}',y_{H1}',0)$ on plane LCD$_1$' is obtained, the fringe pixel value of the same point $A_{RH1}'(x_{H1}',y_{H1}',0)$ on plane LCD1' in plane H can also be calculated. When the x_{H2} value of the point $A_{RH2}(x_{H2},y_{H2},0)$ on plane LCD$_2$ is obtained, the imaging fringe pixel value of the point $A_{RH2}(x_{H2},y_{H2},0)$ on plane LCD$_2$ in plane H can also be obtained.

Because the x value of every point that is imaged in R and H can be calculated, the imaging of the fringe patterns in these two planes can be simulated using Eq. (1).

3.4 Image capture

The resolution of the CCD chip is $X_L \times Y_L$ and the physical size of a single pixel unit on the CCD chip is $d_c \times d_c$. The formula required to calculate the coordinates on the reference plane R based on the coordinates on the projection plane is deduced by the method described in [21]. Because the CCD camera has a similar optical framework to that of a digital light processing projector, the relationship between point A_R on plane R and point A_{RS} on plane S can be obtained using the following equations.

$$\begin{cases} AO = \dfrac{\left(\dfrac{X_L}{2} - X_s\right) \cdot d_c \cdot \dfrac{L}{\cos\theta}}{f \cdot \cos\theta - \left(\dfrac{X_L}{2} - X_s\right) \cdot d_c \cdot \sin\theta} \\[3em] AA_s = \dfrac{\left(Y_s - \dfrac{Y_L}{2}\right) \cdot d_c \cdot \left(AO \cdot \sin\theta + \dfrac{L}{\cos\theta}\right)}{f} \end{cases} \qquad (20)$$

Because $AO = (x - x_o) \times d_M$, $AA_S = (y - y_o) \times d_M$, and Eq. (20) can be rewritten as follows.

$$\begin{cases} X = \dfrac{X_L}{2} - \dfrac{f \cdot (x - x_o) \cdot d_M \cdot \cos\theta}{d_c \cdot \left[(x - x_o) \cdot d_M \cdot \sin\theta + \dfrac{L}{\cos\theta}\right]} \\[3em] Y = \dfrac{Y_L}{2} + \dfrac{(y - y_o) \cdot d_M \cdot f}{d_c \cdot \left[(x - x_o) \cdot d_M \cdot \sin\theta + \dfrac{L}{\cos\theta}\right]} \end{cases} \qquad (21)$$

The coordinate relationship between R and S can be obtained using Eq. (21), and this means that the fringe patterns on plane S can be simulated using the interpolation method.

4. Virtual experiments

4.1 Virtual experimental verification

To verify the validity of the simulated DPMD measurement system, the curved surface formed using a peak function is selected to perform the shape reconstruction process. The parameters related to the CCD camera are as follows: $L=400$ mm, $\theta=25°$, $X_L \times Y_L=2448 \times 2050$, $d_c \times d_c=3.45 \times 3.45$ μm, and $f=35$ mm. The parameters related to the LCD screens are as follows: $d=100$ mm, $\Delta d=40$ mm, $X_{LCD} \times Y_{LCD}=2048 \times 1536$, $d_L \times d_L=96 \times 96$ μm, and the point O$_2$ is set as the center point of screen LCD$_2$. The period P of the fringes is set at 25 pixels. The reference plane size is set at 100 mm×100 mm.

The height distribution of the surface under test is illustrated in Fig. 4. The reflected fringe pattern images corresponding to the reference plane and to the test plane are shown in Fig. 5(a)

and Fig. 5(b), respectively. The captured fringes by the simulated CCD camera that were reflected by plane R and plane H are shown in Fig. 6(a) and Fig. 6(b), respectively. It can be seen that the captured fringes gradually become wider and longer from left to right because of the inclination angle θ. To obtain the phase information from the captured images, a four-step phase-shifting algorithm is used to calculate the wrapped phase. The optimum three-fringe number selection method [22] is used to unwrap the wrapped phase by projection of a series of patterns that have fringe numbers of 81, 80, and 72. After calculation of the unwrapped phase, the height of the test surface can be calculated using Eq. (2). By comparing the calculated height shown in Fig. 7(a) with the preset height, the error distribution can then be obtained, as shown in Fig. 7(b). The root
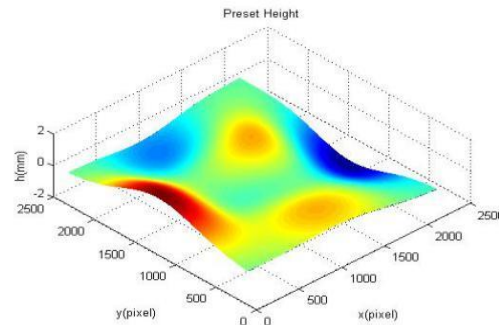
Fig. 4. Height distribution of the test surface.
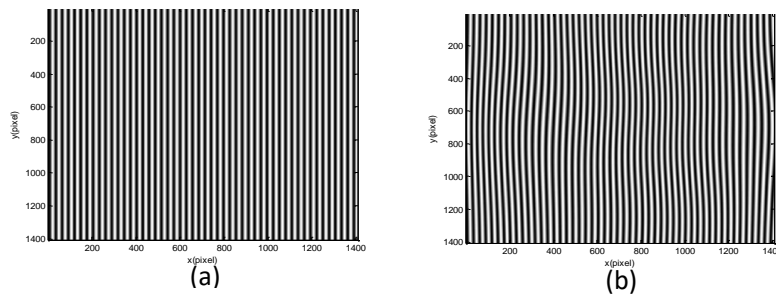
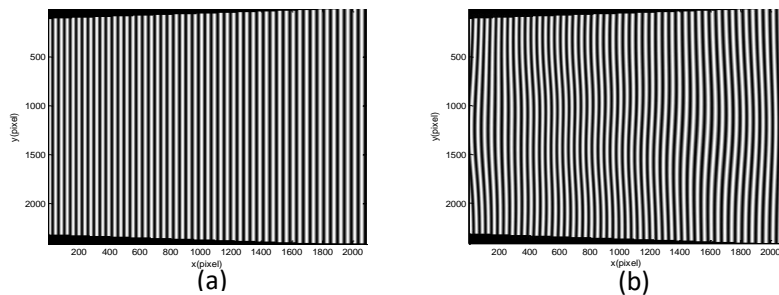Fig. 5. Simulated fringe patterns. (a) Reference plane. (b) Test surface.

Fig. 6. Simulated captured fringe images. (a) Reference plane. (b) Test surface.
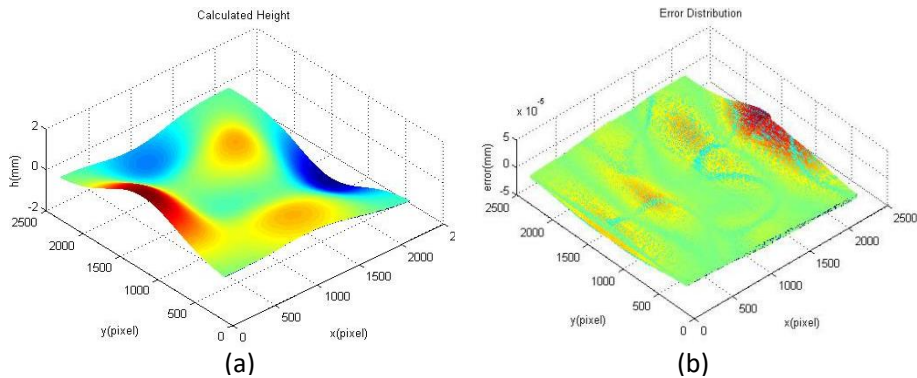

Fig. 7. Height and error distributions. (a) Test surface height distribution. (b) Error distribution.

mean square (RMS) surface error is 1.8077×10^{-5} mm, which demonstrates that the simulated measurement system is both reliable and highly accurate.

4.2 Error analysis using system parameters

Figure 7(b) indicates that the gradient of the surface under test influences the accuracy of the calibration result. When the test plane is a curved surface, the coordinate relationship between the reference plane and the test surface must be calculated via an iterative procedure. To remove the iteration stage, a plane with gradient angles that are all zero is used to simulate the system. The parameter settings of both the CCD camera and the LCD screens are the same as those used in Section 4.1. Point O_2 is set as the center point of screen LCD_2. The reference plane size is set at 80×80 mm. The height of the test plane is set at 10 mm. Gaussian noise with a standard deviation of 3 is added to the gray scale of the original fringe patterns. The system parameters include the distance d between screen LCD_1 and the reference plane, the distance Δd between screen LCD_1' and screen LCD_2, the angle θ between the camera's optical axis and the reference plane, and the fringe period P. To analyze the effects of these four parameters on the measurement results quantitatively, a standard system configuration was chosen as follows: d=100 mm, Δd=40 mm, θ=25°, and P=25 pixels. When the effects of each individual parameter are evaluated, the other three parameters remain constant.

4.2.1 Influence of d

The distance d between screen LCD_1 and the reference plane is varied from 100 mm to 330 mm in increments of 30 mm. Using the simulated measurement system, the relationship between d and the RMS error is obtained as shown in Fig. 8.
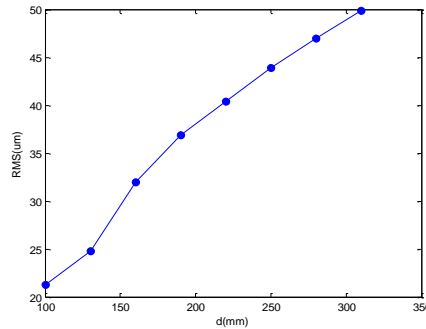

Fig. 8. Relation between d and RMS error.

Figure 8 shows that with increasing d, the RMS error of the measurement results increases gradually. The main reason for this increasing trend is that when the test surface is a plane, the term $(\phi_{r1} - \phi_{r2})$ should be equal to the term $(\phi_{m1} - \phi_{m2})$ in Eq. (8). When the term that includes d is not equal to zero, the error will then increase with increasing d. As d increases, both the distance between phases ϕ_{r1} and ϕ_{m1} and the distance between phases ϕ_{r2} and ϕ_{m2} increase, which improves the signal-to-noise ratio. Figure 8 shows that the error will increase at larger values of d. Therefore, a small d value should be used. In general, d should be no more than 130 mm.

4.2.2 Influence of Δd

The distance Δd between screen LCD_1' and screen LCD_2 is varied from 10 mm to 220 mm in increments of 30 mm. Using the simulated measurement system, the relationship between Δd and the RMS error is then obtained as shown in Fig. 9.

Figure 9 shows that with increasing Δd, the RMS error of the measurement results gradually decreases, and when $\Delta d \geq 40$ mm, the slope over the RMS error range tends to be gentle. The main reason for this trend is that with increasing Δd, both the distance between phases ϕ_{r1} and ϕ_{r2} and the distance between phases ϕ_{m1} and ϕ_{m2} increase, which again improves the

signal-to-noise ratio. Therefore, larger values of Δd should be used. In general, Δd should be no less than 40 mm.
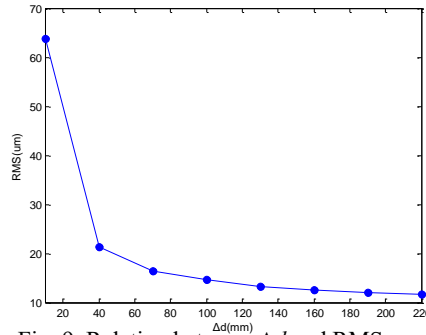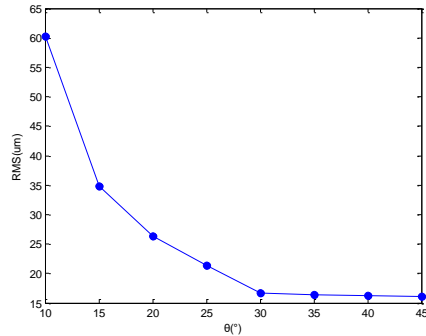

Fig. 9. Relation between Δd and RMS error.

4.2.3 Influence of θ

The angle θ between the optical axis of the camera and the reference plane is varied from 10° to 45° in increments of 5°. Using the simulated measurement system, the relationship between θ and the RMS error is obtained as shown in Fig. 10.

Fig. 10. Relation between θ and RMS error.

Figure 10 shows that with increasing θ, the RMS error of the measurement results gradually decreases. The main reason for this decreasing trend is that with increasing θ, the distances between phases ϕ_{r1} and ϕ_{r2}, phases ϕ_{m1} and ϕ_{m2}, and phases ϕ_{r1} and ϕ_{m1} all increase, which again greatly improves the signal-to-noise ratio. In other words, increasing the angle has the positive effect of inhibiting the noise. However, if the angle of incidence is too large, the camera cannot collect the reflected light. When the test conditions are taken into account, θ should be no less than 25°.
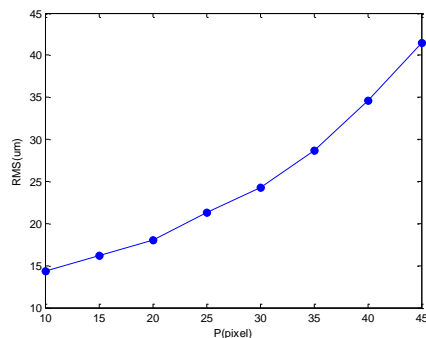
4.2.4 Influence of P

Fig. 11. Relation between P and RMS error.

The period P of the fringe is varied from 10 pixels to 45 pixels in increments of 5 pixels. Using the simulated measurement system, the relationship between P and the RMS error is

obtained as shown in Fig. 11.

Figure 11 shows that with increasing P, the RMS error of the measurement results gradually increases. The main reason for this trend is that with increasing P, the distance between the adjacent phase fringes on the LCD screen increases, which then improves the signal-to-noise ratio. Figure 11 also shows that while the reduction of P has an inhibitory effect on the noise overall, this effect is not obvious. Consequently, the value of P is reasonable when it is no more than 25 pixels.

4.2.5 Influence of parallelism

The inclination angle α_1 between the reference plane and the two LCD screens are varied from 0.05 degrees to 0.25 degrees in increments of 0.05 degrees. Using the simulated measurement system, the relationship between α_1 and the RMS error is obtained as shown in Fig. 12. The same procedure has been applied to the inclination angle α_2 between the two LCD screens. Figure 13 shows the relationship between α_2 and the RMS error.
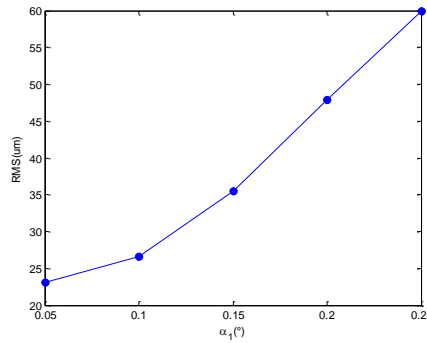

Fig.12 Relation between α₁ and RMS

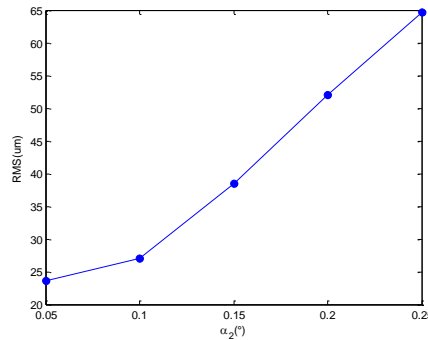Fig.13 Relation between α₂ and RMS

Figures 12 and 13 show that with increasing inclination angles α_1 and α_2, the RMS error of the measurement results increases gradually. The main reason for this trend is that with the increasing α_1 and α_2, the deviation between the two measured parameters d, Δd and the true value is larger along x direction. Therefore, a small inclination angle α_1 and α_2 value should be guaranteed in actual measurements. In general, both of them should be no more than 0.15 degrees.

5. Actual experiments and discussion

5.1 Hardware system

To verify the simulated results, actual experiments were performed. To simplify the experimental process while also ensuring the measurement accuracy, the realization of two parallel LCD screens is dependent on moving one of the LCD screens to two different positions using a linear translation stage. The experimental system is shown in Fig. 14, and includes a CCD camera, an LCD screen, three linear translation stages and a mirror. The camera is model eco655CVGE from SVS (Bremen, Germany) and has a resolution of 2448×2050 px. The LCD

screen is model LP097QX2 from LG (Seoul, Korea) and has a resolution of 2048×1536 px. The three automatic translation stages, which have model numbers of GCD-203300M, GCD-203300M and GCD-203200M, are all from Daheng New Epoch Technology Inc (Beijing, China) and have the same accuracy of 1 μm. The LCD screen, the reference mirror and the CCD camera were fixed on the first, second and third automatic translation stages, respectively.
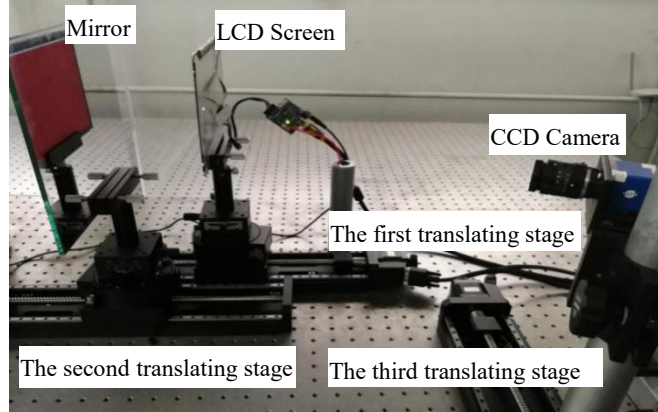

Fig. 14 Hardware setup for the measurement system.

5.2 Experimental process and results

First, the imaging system hardware was positioned accurately using the given parameters. When the LCD screen was in the first position, the deformed fringe pattern that was reflected by the mirror that was used as the reference surface was then captured by the CCD camera. Second, the mirror was moved by 10 mm using the second stage and was then used as the test surface. The deformed fringe pattern that was reflected by the mirror was then captured by the CCD camera. Third, the LCD screen was moved by Δd to the second position by the first stage. The deformed fringe pattern that was reflected by the mirror was again captured using the CCD camera. Fourth, the mirror was moved back to its original position and was then used as the reference surface. The deformed fringe pattern that was reflected by the mirror was again captured by the CCD camera. The distance between the mirror that was used as the reference surface and the mirror that was used as the test surface was 10 mm, and thus the height of the test surface was 10 mm. When the test surface height was obtained, the RMS error could then be calculated. The standard configuration for the actual measurement system was chosen to be d=102.5 mm, Δd=40 mm, θ=24.9°, and P=25 pixels. When the effects of each individual parameter were evaluated, the other three parameters remained unchanged. The experimental results are shown in Fig. 15.

Figure 15(a) shows the influence of the measurement errors for four different values of d: 102.5 mm, 132.5 mm, 152.5 mm, and 177.5 mm. With increasing d, the RMS errors of the measurement results increase gradually, which is the same trend as in the simulated results described earlier. Therefore, small values of d should be applied.

Figure 15(b) similarly demonstrates the influence of the measurement errors for four different values of Δd: 10 mm, 25 mm, 40 mm, and 75 mm. With increasing Δd, the RMS errors of the measurement results gradually decrease, which is the same trend as in the simulated results described earlier. Therefore, a large value of Δd should also be applied.

Figure 15(c) demonstrates the effects of the measurement errors for four values of θ: 16.7°, 19.1°, 24.9°, and 28.1°. With increasing θ, the RMS errors of the measurement results gradually decrease, which is again the same trend as in the simulated results described earlier. A small value of θ should thus be applied accordingly. Additionally, it should be guaranteed that the reflected

light can be collected by the camera.

Figure 15(d) demonstrates the influence of the measurement errors for four different values of parameter P: 20 pixels, 25 pixels, 32 pixels, and 41 pixels. With increasing P, the RMS error of the measurement results gradually increases, which is the same trend as in the simulated results given above. Therefore, a small value of P should be used. In general, P should be no more than 25 pixels. Additionally, to maintain the sinusoidal topography of the fringes and guarantee that the camera can distinguish these fringes, P should also be no less than 16 pixels.
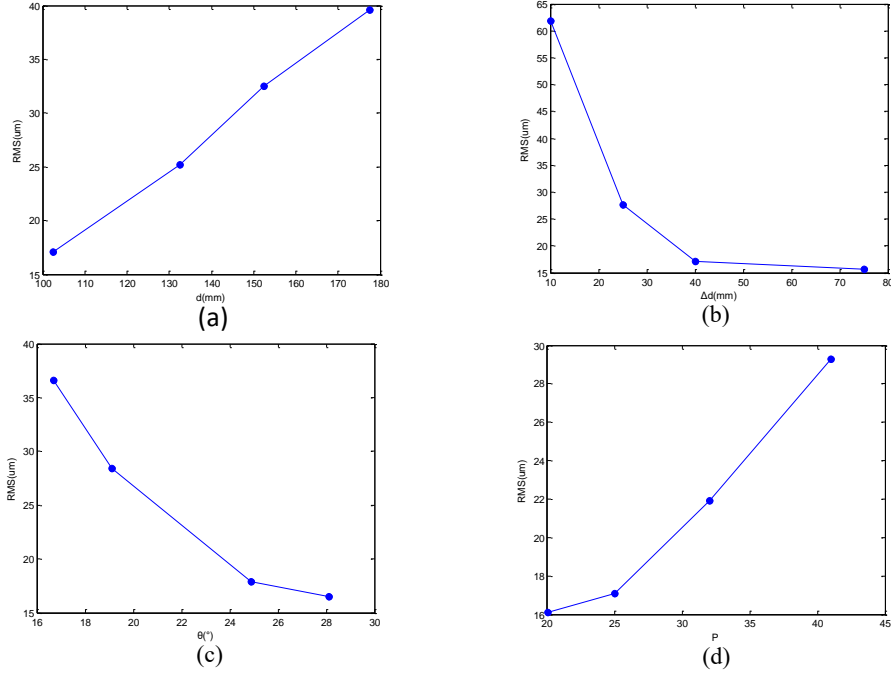

Fig. 15. Relationships between parameters and RMS error. (a) d and RMS error, (b) Δd and RMS error, (c) θ and RMS error, and (d) P and RMS error.

Another evaluation experiment was performed by measuring a manufactured artificial step with multiple discontinuous specular surfaces, as shown in Fig. 16(a). When the influence of the system parameters on the measurement results was taken into account, $d = 102.5$ mm, $\Delta d = 40$ mm, $\theta = 25°$, and $P = 25$ pixels. The step is shown with projected red fringes in Fig. 16(b). The absolute phase map and the measured 3D shape data are shown in Fig. 16(c) and 16(d), respectively.

To evaluate the measurement system accuracy quantitatively, the actual distance between neighboring steps was measured using a coordinate measurement machine (CMM). To calculate the distances between neighboring steps, all measured points on a single step surface were fitted into a plane. The measured distance between neighboring steps was calculated using the average distance value for all points obtained on the other step surface to the fitted plane. The actual distance, the measured distance, the absolute error (i.e., the absolute difference between the measured average distance and the actual distance) and the standard deviation are all listed in Table 1. The maximum absolute error and the maximum RMS error are 0.023 mm and 0.023 mm, respectively. These experimental results demonstrate that the proposed measurement system can obtain the required depth data with high precision and high reliability.
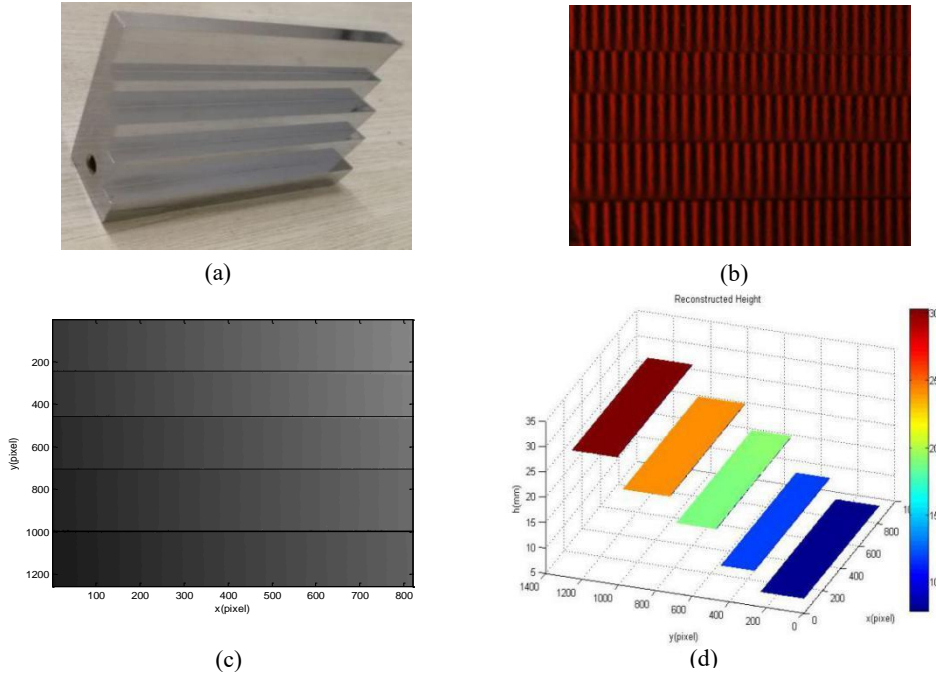
Fig. 16. Illustration of manufactured step and measured 3D shape data. (a) Manufactured step; (b) captured fringe on the step; (c) absolute phase map; and (d) measured 3D shape.

Table 1. Experimental results on the tested step (units: mm).

Actual distance	Measured distance	Absolute error	RMS
3.987	3.964	0.023	0.023
7.025	7.043	0.018	0.012
5.006	4.987	0.019	0.021
6.099	6.115	0.016	0.020

6. Conclusions

A novel virtual measurement system has been developed based on a direct phase measuring deflectometry (DPMD) technique. The effects of the four system parameters on the measurement results have been analyzed and the performance of the proposed measurement system was evaluated. Simulated and actual experiments were carried out. The results showed that with increasing distance Δd between the two LCD screens, the angle θ between the camera's optical axis and the reference mirror, the RMS errors of the measurement results decrease gradually. However, with increasing distance d between the LCD1' screen (virtual image of screen LCD1) and the reference mirror, the period P of the fringe pattern, the RMS error of the measurement results gradually increase. Therefore, suitable system parameters can be selected for the actual DPMD measurement system to obtain the 3D shape of a specular object with high accuracy.

References

[1]Zhang Z H. Review of single-shot 3D shap measurement by phase calculation-based fringe projection techniques. Opt Lasers Eng 2012;50:1097-1106.

[2]Xu J, Liu S L, Wan A, Gao B T, Yi Q, Zhao D P, et al. An absolute phase technique for 3D profile measurement using four-step structured light pattern. Opt Laser Eng 2012;50:1274-1280.

[3]Zuo C, Chen Q, Gu G, Feng S, Feng F. High-speed three-dimensional profilometry for multiple objects with complex shapes. Opt Express 2012;20:19493-19510.

[4]Cai Z W, Liu X L, Peng X, Yin Y K, Wu J C, Gao B Z, et al. Structured light field 3D imaging. Opt Express 2016;24:20324-20334.

[5]Xu J, Xi N, Zhang C, Zhao J G, Gao B T, Shi Q. Rapid 3D surface profile measurement of industrial parts using two-level structured light patterns. Opt Lasers Eng 2011;49:907-914.

[6]Liu X L, Peng X, Chen H L, He D, Gao B Z. Strategy for automatic and complete three-dimensional optical digitization. Opt Lett 2012;37:3126-3128.

[7]Fang F Z, Zhang X D, Weckenmann A, Zhang G X, Evans C. Manufacturing and measurement of freeform optics. CIRP Ann-Manuf Techn 2013; 62:823-846.

[8]Su P, Parks R E, Wang L, Angel R P, Burge J H. Software configurable optical test system: a computerized reverse Hartmann test. Appl Opt 2010;49:4404-12.

[9]Maldonado A V, Su P, Burge J H. Development of a portable deflectometry system for high spatial resolution surface measurements. Appl Opt 2014;53:4023-4032.

[10]Huang L, Ng C S, Asundi A K. Dynamic three-dimensional sensing for specular surface with monoscopic fringe reflectometry. Opt Express 2011;19:12809-12814.

[11]Tang Y, Su X Y, Liu Y K, Jing H L. 3D shape measurement of the aspheric mirror by advanced phase measuring deflectometry. Opt Express 2008;16:15090-15096.

[12]Tang Y, Su X Y, Wu F, Liu Y K. A novel phase measuring deflectometry for aspheric mirror test. Opt Express 2009;17:19778-19784.

[13]Xiao Y L, Su X Y, Chen W J. Flexible geometrical calibration for fringe-reflection 3D measurement. Opt Lett 2012;37:620-622.

[14]Petz M,Tutsch R. Reflection grating photogrammetry: a technique for specular reflection surfaces. Proc. Of SPIE 2005;58691:D1-D12.

[15]Guo H W, Peng F, Tao T. Specular surface measurement by using least squares light tracking technique. Opt Lasers Eng 2010;48:166–171.

[16]Knauer M C, Kaminski J, Häusler G. Phase measuring deflectometry: a new approach to measure specular free-form surfaces. Proc. SPIE 2004;5457:366-376.

[17]Feng S J, Chen Q, Zuo C, Asundi A. Fast three-dimensional measurements for dynamic scenes with shiny surfaces. Opt Commun 2017;382:18-27.

[18]Huang L, Xue J P, Gao B, Mcpherson C, Beverage J, Idir M. Modal phase measuring deflectometry. Opt Express 2016;24:24649-24664.

[19]Liu Y, Huang S J, Zhang Z H, Gao N, Gao F, Jiang X Q. Full-field 3D shape measurement of discontinuous

specular objects by direct phase measuring deflectometry. Sci Rep, Accepted.

[20] Zhang Z H, Zhang D, Peng X. Performance analysis of a 3D full-field sensor based on fringe projection. Opt Lasers Eng 2004;42:341-353.

[21] Zhou D, Wang Z Y, Gao N, Zhang Z H. Virtual fringe projection system with nonparallel illumination based on iteration. Meas Sci Technol 2017;doi:10.1088/1361-6501/aa6597.

[22] Zhang Z H, Towers C E, Tower D P. Time efficient color fringe projection system for 3D shape and color using optimum 3-frequency selection. Opt Express 2006;14:6444-55.